

## Research Article

# Numerical Analysis of Bubble Formation Mechanism in Nucleate Pool Boiling

\*<sup>1</sup>E. Koç , <sup>1</sup>İ. Y. Uralcan 

<sup>1</sup>Istanbul Technical University, Department of Mechanical Engineering, Istanbul, Turkey  
E-mail: \*esraunver@itu.edu.tr

Received 23 March 2025, Revised 20 April 2025, Accepted 8 May 2025

### Abstract

This study comprehensively investigates nucleate pool boiling by focusing on bubble formation, growth, and detachment mechanisms. A numerical analysis of saturated nucleate pool boiling of water on a heated surface, specifically emphasizing a single cavity, was conducted and compared with experimental results documented in the literature. Accurate modeling of boiling phenomena is crucial, particularly in effectively capturing the mass transfer and phase change processes between the liquid and vapor phases. The dynamic separation of these phases through a moving interface presents a significant challenge when simultaneously applying the Navier–Stokes equations to both phases, as it complicates the continuity conditions at the interface. Various numerical methods, incorporating implicit and explicit schemes, have been developed to address these challenges for two-phase flow simulations. Interface tracking techniques such as the Volume of Fluid (VOF), Level-Set, and Lattice Boltzmann methods are commonly employed. This study used Ansys Fluent software to perform a detailed boiling model analysis. Based on the findings from detailed literature reviews, the Volume of Fluid (VOF) method is considered the most suitable simulation approach for modeling pool boiling. After establishing an appropriate computational domain, a two-dimensional simulation of single bubble formation on a microscale heated surface was carried out using a custom-developed User Defined Function (UDF). The objective was to analyze the bubble's geometric characteristics and diameter evolution throughout the boiling process. The accuracy of the numerical model was evaluated by comparing simulation results with experimental observations reported in the literature, showing a high degree of agreement. CFD analyses were conducted for both a flat copper surface and a surface with a single cavity. The results showed that, due to nucleate boiling, the copper surface's superheat values were higher than those on the surface with a cavity. This indicates improved heat transfer performance on the structured surface. These findings suggest that in processes where boiling-induced heat transfer is applied, surfaces that are roughened either through etching or coating methods may yield enhanced thermal performance compared to smooth surfaces, in line with observations reported in the literature.

**Keywords:** Nucleate pool boiling; bubble dynamics; two-phase simulation; VOF; UDF; CFD.

### 1. Introduction

Numerical modeling is a powerful tool that complements and accelerates experimental investigations in boiling heat transfer. This study numerically examines bubble formation, growth, and detachment within a single cavity during saturated nucleate pool boiling on a heated surface. The simulation results are compared with experimental data to validate the numerical approach. Boiling-induced phase change at the heated surface results in substantial heat flux, making it a critical process in thermal systems. Although several semi-empirical models have been developed to describe the underlying physical mechanisms of boiling, many aspects remain inadequately understood, limiting their applicability to specific conditions.

Boiling heat transfer is widely utilized across various industries due to its capacity to achieve high heat transfer rates with relatively low temperature differences. Pool Boiling Heat Transfer (PBHT) is critical in multiple industrial applications due to its high heat transfer efficiency. These include energy systems, electronics cooling, nuclear reactors, and waste heat recovery units. The morphological

characteristics and wettability of heating surfaces directly affect the efficiency of such systems. In recent years, research on surface modification to enhance boiling performance has gained considerable momentum [1]. Over the years, numerous experimental and computational studies have been conducted to unravel the complex nature of boiling phenomena at microscopic and macroscopic scales. These efforts have focused on fundamental processes such as nucleation, bubble growth and collapse, oscillation, detachment, and interactions among adjacent bubbles. Recent efforts have focused on enhancing pool boiling heat transfer by modifying surface structures and using advanced working fluids [2]. Enhancing nucleate pool boiling is crucial for improving thermal system efficiency, and one promising approach involves using nanofluids, base fluids enhanced with nanoparticles to improve thermal conductivity and boiling performance [3].

A central theme in boiling research is the detailed analysis of the complete life cycle of individual vapor bubbles and their interactions, as these significantly influence overall heat transfer performance. In particular,

bubble coalescence has been identified as a significant factor affecting fluid motion and thermal transport during pool boiling. The merging of bubbles promotes the evaporation of the liquid layer entrapped between their bases, thereby enhancing heat transfer [4], [5].

Despite extensive research, the physical mechanisms governing boiling have not yet been fully elucidated, and a comprehensive theoretical model has yet to be developed. For theoretical approaches, both analytical and numerical, to be reliable, these mechanisms must be clearly defined and accurately represented.

## 2. Literature Review

Boiling is the evaporation process at the solid–liquid interface [6]. It is initiated when the temperature of the heated surface ( $T_w$ ) exceeds the saturation temperature ( $T_{sat}$ ) of the liquid at a given pressure. Newton’s law of cooling commonly expresses the heat flux per unit area during boiling as the following equation [6]:

$$q'' = h(T_w - T_{sat}) = h\Delta T_e \quad (1)$$

Where  $q''$  is the heat flux,  $h$  is the convective heat transfer coefficient, and  $\Delta T_e$  is the excess temperature or superheat, representing the temperature difference between the heated surface and the saturated liquid. The boiling process encompasses several fundamental mechanisms, including nucleation, bubble growth, coalescence, and detachment, which significantly influence heat transfer performance.

Hsu [7] contributed to understanding these mechanisms by identifying four distinct stages in the bubble emission cycle during nucleate boiling. In the first stage, a vapor bubble initiates growth at a nucleation site due to localized superheating, overcoming surface tension forces that initially inhibit phase change. This is followed by forming a microlayer- a thin liquid film beneath the growing bubble-critical in enhancing heat transfer through rapid evaporation. As the bubble grows, surface tension governs its shape while buoyancy drives its upward movement. Finally, bubble departure occurs when the buoyant force exceeds the adhesive forces anchoring the bubble to the surface, determining its detachment size and concluding the growth cycle.

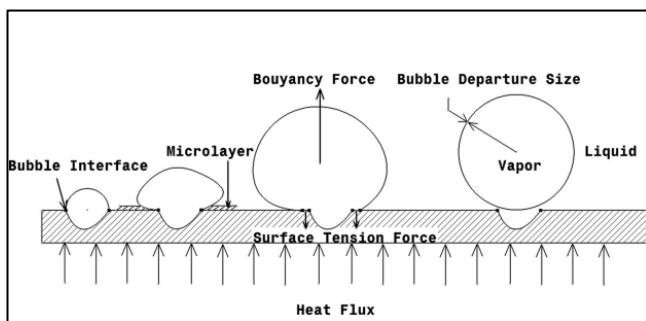


Figure 1. Stages of bubble formation and growth [8].

These sequential stages define the bubble life cycle in nucleate boiling and serve as a foundational framework for analyzing heat transfer dynamics in such systems. Figure 1 illustrates the stages of bubble formation and growth, depicting the progression from initial nucleation to final bubble detachment, as detailed [8].

According to Kenning [9], the bubble detaches from the heated surface following the growth phase, disrupting the

thermal boundary layer and allowing cooler liquid from the surrounding bulk to replenish the vacated space. Once the thermal boundary layer recovers, a new nucleation cycle is initiated. The time required for the thermal boundary layer to re-establish itself is called the *holding time*.

Paruya et al. [10] developed a model that incorporates the effects of the microlayer, utilizing the Young–Laplace equation for both low and high superheat conditions. Their model was compared with Computational Fluid Dynamics (CFD) results from existing literature and their experimental data. The comparison demonstrated strong agreement, indicating that the proposed model accurately captures the bubble growth and detachment dynamics.

Petrović et al. [11] introduced the Grid-Resolved Wall Boiling Model (GRWBM) as an enhancement over traditional CFD methods for simulating nucleate boiling. In contrast to the commonly used Subgrid Wall Boiling Model (SWBM), GRWBM explicitly differentiates between bubble growth sites and the remaining heated wall surface during conjugate heat transfer to the liquid. Validation against detailed experimental datasets showed that GRWBM offers improved predictions under high heat flux conditions, particularly in capturing transient wall temperature fluctuations, average wall superheat, void fraction distribution along the pool height, and the swelling behavior of the two-phase mixture.

Iyer et al. [12] proposed a comprehensive pool boiling model encompassing the entire bubble life cycle from nucleation to detachment. The model comprises three interrelated components: heat transfer, force acting on bubbles, and evolution of bubble shape. A novel feature of this approach is the representation of bubbles as truncated spheres atop conical bottlenecks. Validation through CFD simulations and experimental observations confirmed the model’s reliability, with good agreement observed regarding bubble lift-off time, wall temperature, bubble morphology, and microlayer thickness, as reported in existing literature.

Mahmoud et al. [13] conducted an experimental investigation to measure the bubble growth rate during saturated pool boiling of deionized water on a smooth copper surface at atmospheric pressure. A smooth surface was intentionally selected to minimize uncertainties arising from surface microstructure effects on bubble dynamics. The measurements were restricted to the isolated bubble regime, and comparisons with existing bubble growth models revealed that the bubble growth rate and exit diameter increased with rising wall superheat.

In the Al-Nagdy et al. [1] study, microchannels with widths ranging from 200 to 1000  $\mu\text{m}$  were fabricated on stainless steel surfaces using laser processing and tested under heat fluxes between 10 and 150  $\text{kW}/\text{m}^2$ . Results showed that narrower microchannels notably enhanced the heat transfer coefficient (HTC), with a maximum improvement of 94.3% at 200  $\mu\text{m}$  width. Response Surface Methodology (RSM) was employed to optimize the system parameters, identifying an optimal HTC of 43.93  $\text{kW}/\text{m}^2\text{K}$  at a 217  $\mu\text{m}$  channel width and 146  $\text{kW}/\text{m}^2$  heat flux. These findings demonstrate the effectiveness of laser-textured surfaces and statistical modeling in improving nucleate pool boiling performance.

Eid et al.’s study [2] investigates the effects of laser-fabricated micro-cavities, cylindrical, cubic, and pentagonal, on the heat transfer performance of brass heating surfaces. Furthermore, the impact of aluminum oxide ( $\text{Al}_2\text{O}_3$ ) nanoparticles suspended in water is analyzed to evaluate

combined enhancement techniques. Experimental results demonstrate that geometric cavity design significantly improves heat transfer coefficients (HTC), with pentagonal cavities achieving up to 123.4% enhancement in pure water and 140.5% in nanofluid at low concentrations. These findings confirm that surface structuring and nanofluid additives boost nucleate boiling performance.

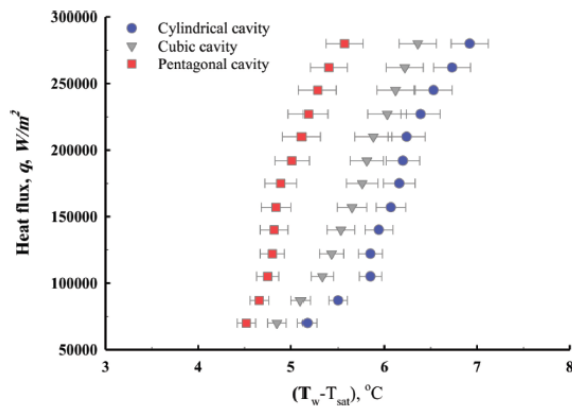


Figure 2. Pool boiling curve of pure water for different structured surfaces [2].

Figure 2 illustrates the variation of wall superheat temperature as a function of the applied heat flux for different micro-cavity geometries. In this context, the heat flux is calculated based on each micro-structured heating surface's projected (planar) area. Wall superheat, denoted as the temperature difference between the actual surface temperature at the top of the micro-cavity and the saturation temperature of water under atmospheric pressure, is a key parameter in evaluating boiling performance. A noticeable leftward shift in the boiling curves for the modified surfaces indicates a substantial reduction in wall superheat, which directly correlates with improved boiling heat transfer characteristics. Specifically, the cylindrical, cubic, and pentagonal micro-cavity surfaces exhibited reductions in wall superheat of 45.4%, 48.5%, and 55.2%, respectively, compared to the smooth (mirror-finished) reference surface. These reductions confirm that modifying the surface geometry with precise micro-cavities can significantly enhance nucleation activity and reduce the thermal resistance at the liquid–solids interface, thereby promoting more efficient phase change heat transfer [2].

Eid et al.'s study [3] focuses on the influence of aluminum oxide ( $\text{Al}_2\text{O}_3$ ) nanoparticles suspended in refrigerant R-134a on pool boiling heat transfer. Experiments were conducted using a stainless-steel cylindrical heater with varying surface roughness, nano concentrations, and operating pressures. The results demonstrate that incorporating  $\text{Al}_2\text{O}_3$  nanoparticles significantly enhances the heat transfer coefficient (HTC), particularly at lower concentrations and higher surface roughness levels. The maximum HTC enhancement reached 167.7%, while higher nanoparticle concentrations led to a performance decline due to surface deposition effects. An empirical correlation was also proposed to predict HTC based on key parameters, including pressure, heat flux, particle concentration, and surface texture. These findings highlight the effectiveness of nanofluids and surface engineering in advancing boiling heat transfer applications [3].

Alsaati et al. [14] developed a mechanical model to predict the Critical Heat Flux (CHF) during narrow-range

boiling in a separate study. The model is based on the irreversible growth of the dry spot, driven by the interplay of vapor recoil, surface tension, and hydrostatic forces. CHF initiation occurs when the vapor recoil force from intense evaporation counterbalances the combined effects of surface tension and hydrostatic pressure, leading to sustained dry spot expansion. The model, called the predictive trapped CHF model, incorporates parameters such as confinement geometry, operating temperatures, and CHF characteristics. Although it does not strictly align with traditional CHF conditions in near-evaporation cooling gaps, it effectively estimates the threshold range for pool boiling CHF, offering a practical tool for prediction and control.

Qiu et al. [15] investigated microlayer evaporation in nucleate pool boiling under varying pressure conditions. They developed an analytical method for estimating initial microlayer thickness and validated it through experiments at different pressures. For cases involving multiple bubbles, a nucleation site tracking approach was applied. The complete multi-bubble evaporation model was compared with high-pressure pool boiling experiments, yielding strong agreement with experimental data. Their findings underscore the crucial role of the microlayer in vapor generation and reveal that increasing pressure significantly reduces microlayer evaporation, highlighting the sensitivity of interfacial phase change to operating conditions.

Kumar et al. [16] introduced a physics-based model to improve predictions of bubble departure diameter in nucleate pool boiling. The model employs a force balance analysis, accounting for buoyancy, surface tension, and pressure differential forces. A new coefficient specific to water is introduced, enabling more accurate estimation of departure diameter based on the Jacob number and contact angle. The model was validated against five experimental datasets and compared with five existing models. Results demonstrated superior predictive accuracy, with maximum and minimum average absolute deviations of 30% and 14%, respectively, and 90% of literature data falling within a  $\pm 25\%$  error margin.

Kim and Kim [17] proposed a mechanistic nucleate pool boiling heat transfer model incorporating the influence of bubble coalescence. They analyzed transient temperature and heat flux distributions across the boiling surface using high-speed infrared imaging, categorizing surface regions into natural convection, quenching, and evaporation zones. While bubble coalescence was found not to alter heat flux values significantly, it did affect the area fraction of each region. A new heat flux correlation was formulated and validated using experimental data for water and FC-72. The model demonstrated improved predictive accuracy, particularly in capturing the heat flux change rate with wall superheat, reducing error by 94% compared to models that neglect coalescence effects.

Yuan et al. [18] conducted a numerical investigation utilizing the phase-change Lattice Boltzmann Method (LBM) to simulate the spontaneous nucleation and interaction of individual vapor bubbles, with the model incorporating an equation of state to capture phase change phenomena. As stated in their study, the simulation setup involved two identical micro-heaters with a specified wall superheat of  $5^\circ\text{C}$  and a separation distance of 28 lattice units. This configuration enabled the generation of two identical bubbles and allowed for a detailed examination of their growth and coalescence dynamics. The results were compared against experimental observations reported by

Mukherjee and Dhir [19], providing a means of qualitative validation.

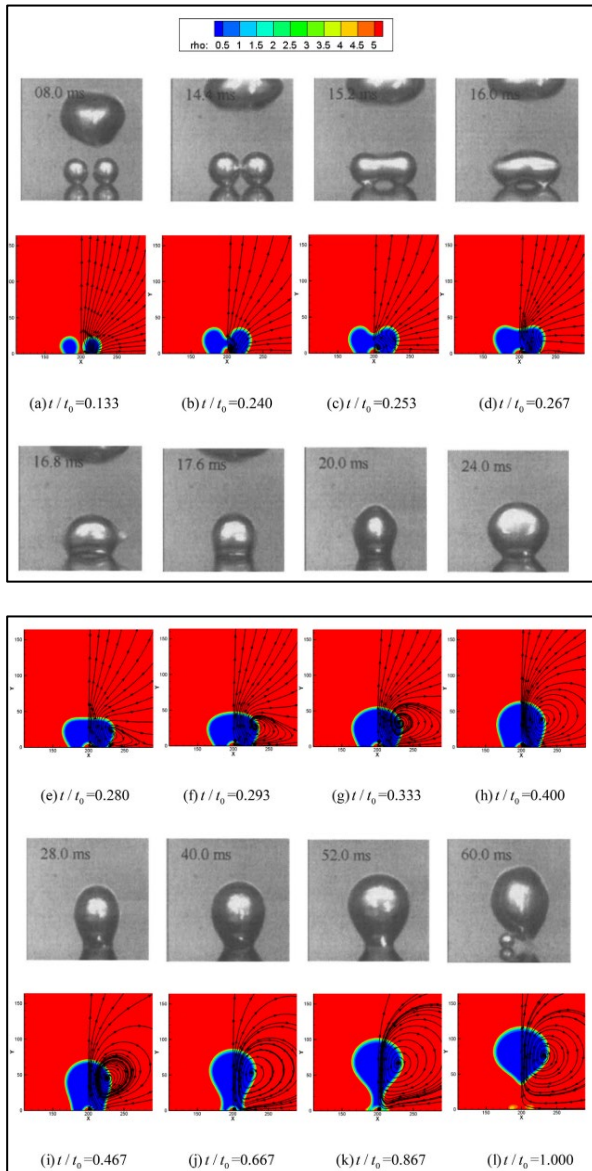


Figure 3. Numerical simulation results and corresponding experimental observations of a representative ebullition cycle involving bubble coalescence during nucleate boiling at a wall superheat of 5 °C [19].

The computational domain was designed to be symmetrical, and the right half of the flow field was visualized over the simulated density distribution. Initially, bubble nuclei emerged at the centers of the two micro-heaters and underwent gradual growth (Figure 3a). As the bubbles expanded and their interfaces came into contact, coalescence was initiated (Figure 3b). This contact led to the rupture of the interface and the formation of a vapor bridge connecting the two bubbles (Figure 3c). A supplementary microlayer was observed forming beneath this vapor bridge (Figure 3c and 3d), which significantly enhanced local heat transfer at the wall due to its relatively lower temperature.

The presence of this microlayer led to the generation of strong vortices beneath the bubble structure. Additionally, surface tension forces acting on the vapor bridge pulled the two bubbles together, eventually resulting in a single, merged bubble (Figure 3e). At this stage, the supplementary microlayer was seen to be trapped within the bubble, and a pair of vortices formed symmetrically on either side.

Following coalescence, the merged bubble exhibited oscillatory deformation: it first elongated vertically along the Y-direction due to inertial effects and then expanded laterally in the X-direction as surface tension took over (Figure 3f–3i). Eventually, the bubble necked and detached from the heated surface under the influence of buoyant forces (Figure 3j–3l), with the associated vortices rising alongside it. Overall, the predicted bubble behavior closely matched experimental observations, capturing all major phases of a typical ebullition cycle involving coalescence: nucleation and individual growth, bubble coalescence, post-coalescence oscillation and expansion, and final detachment. The study notably highlighted the key roles of microlayer dynamics and vortex formation in the heat transfer and bubble departure.

In light of all these studies, simulations were conducted on a single-cavity copper plate, designed as smooth and etched surfaces under varying heat flux conditions. In this way, results regarding bubble growth rate and diameter at different heat flux levels were obtained, which can be compared with findings reported in the literature.

### 3. Numerical Model

The modeling process in this study is guided by a set of assumptions to simplify and accurately represent the physical phenomena involved. The system consists of two interacting phases, liquid water and water vapor, where bubble formation occurs at a conical cavity on the heated surface.

Table 1. Thermophysical properties of liquid water and vapor at 373.15 K.

Property	Unit	Water	
		Liquid	Vapor
Density, $\rho$	kg/m <sup>3</sup>	958	0.597
Specific heat, $C_p$	J/kg·K	4220	2030
Thermal conductivity, $k$	W/m·K	0.679	0.025
Viscosity, $\mu$	Pa·s	$2.77 \times 10^{-4}$	$1.30 \times 10^{-5}$
Latent heat of vaporization, $h_{fg}$	kJ/kg	2256	
Surface tension, $\sigma$	N/m	0.059	
Saturation temperature, $T_{sat}$	K	373.15	
Pressure, $P$	MPa	1.013	

The liquid in the pool is assumed to remain at the saturation temperature throughout the boiling process, ensuring thermal equilibrium in the bulk fluid. Boiling is initiated and sustained by constant heat flux to the heated surface. These assumptions establish a controlled environment for analyzing the fundamental mechanisms of nucleate boiling, particularly the dynamics of bubble formation, growth, and departure under idealized thermal and geometric conditions.

The pool initially contains water at a temperature of 373.15 K; the thermophysical properties are given in Table 1. During the simulation, the thermophysical properties of both liquid water and water vapor, such as specific heat, thermal conductivity, and viscosity, are assumed to vary with temperature. Additionally, surface tension forces and buoyancy forces resulting from the density difference between phases are included in the model. These forces are critical for accurately representing dynamic processes such

as bubble detachment from the surface and its upward motion [3].

Table 2 presents the thermophysical properties of copper, which is the solid material used in the constant heat flux boundary condition.

Table 2. Thermophysical properties of copper at 373.15 K.

Property	Unit	Copper
Density, $\rho$	kg/m <sup>3</sup>	8920
Specific heat, $C_p$	J/kg·K	385
Thermal conductivity, $k$	W/m·K	391

In Figure 4, the ANSYS Fluent model employed in this study is a two-dimensional axisymmetric representation of the experimental setup designed to simulate a single cavity. The computational domain comprises two distinct regions: a solid region representing copper and a fluid region representing water.

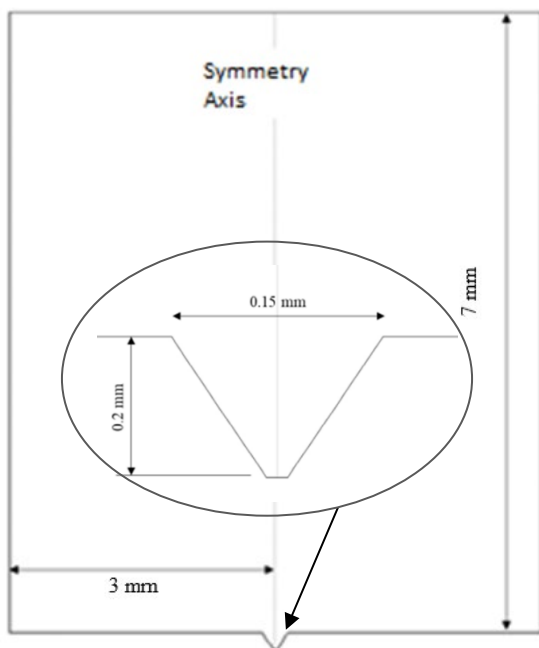


Figure 4. The geometry and dimensions of the cavity where the analyses are conducted.

Material properties corresponding to copper are assigned to the solid domain, while the thermophysical properties of water are specified for the fluid domain. A conical cavity, with a mouth diameter of 150  $\mu\text{m}$  and a depth of 200  $\mu\text{m}$ , is incorporated into the boiling surface to serve as the nucleation site. Bubble formation is confined to this cavity, and the complete bubble nucleation cycle encompassing growth and departure is analyzed over time to investigate the dynamics of nucleate boiling under controlled conditions.

In Figure 5a, the boundary conditions of the CFD model are given. The flow domain was modeled as axisymmetric, with the axis of symmetry selected as the centerline of the domain. An adiabatic boundary condition was applied to the sidewalls of the pool. The inlet and outlet boundary conditions were defined as constant heat flux and atmospheric pressure (pressure outlet), respectively. The mesh model of the cavity is shown in Figure 5b a cylindrical region with a diameter of 1.2 mm was defined above the cavity, and hexagonal elements with a side length of 0.025 mm were used throughout the flow domain. In regions near the cavity where all three phases coexist, the mesh was

refined using hexagonal elements with a size of 0.01 mm. To reduce computational time, quadrilateral and hexagonal elements with a size of 0.05 mm were employed in the remaining areas.

In the mesh quality evaluation, highly favorable results were obtained according to various quality criteria. The Jacobian value was measured as 0.98, which is very close to the ideal value of 1, indicating a high-quality mesh structure. The aspect ratio was 1.01, also near the ideal value of 1, suggesting that the mesh cells are proportionally distributed.

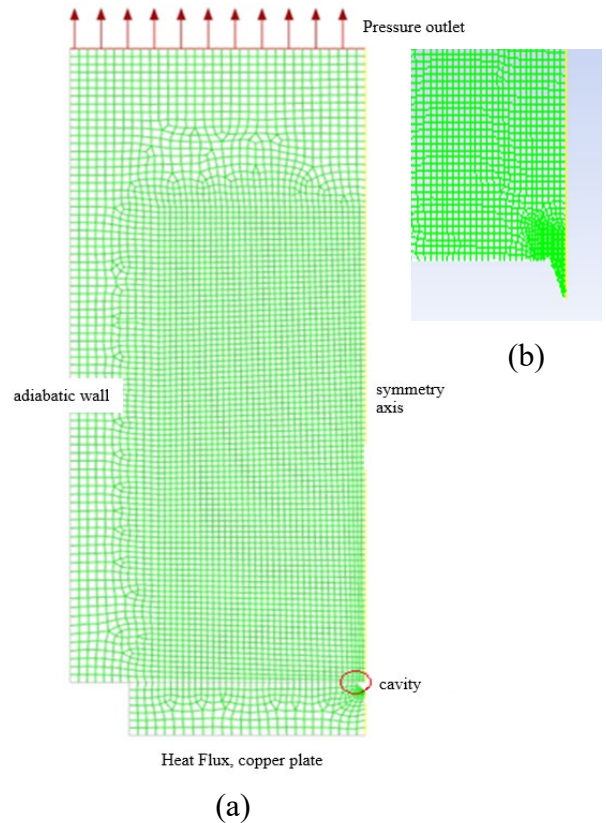


Figure 5. a) Boundary condition of the CFD model, b) Mesh model at the cavity.

The orthogonal quality value was recorded at 0.994, which is considered nearly perfect and reflects that the cells are connected at almost orthogonal angles. Regarding skewness, the minimum value was found to be  $1.9 \times 10^{-6}$ , which is excellent, while the maximum value was 0.515, slightly above the commonly accepted threshold. However, this suggests that only a few cells exhibit minor distortion and that the mesh structure remains unaffected. Overall, the mesh is of high quality and is suitable and reliable for numerical analysis [20].

In numerical modeling studies, it is essential to ensure that the results are independent of the mesh structure and consistent with experimental data to develop reliable models. Mesh independence tests are conducted by altering the number, size, and geometry of mesh elements to evaluate whether the resulting outputs fall within acceptable error margins [21].

In this study, three different mesh structures were generated by varying the number of nodes and elements, and analyses were conducted for the equivalent diameter of bubble growth. The number of nodes and cells for each mesh structure is presented in Table 3.

The equivalent diameter is a spherical diameter determined solely based on the vapor volume, independent of the actual geometry of the bubble, and is expressed by the following relation [22]:

$$D_{eq} = \left( \frac{6 \cdot V_{vapor}}{\pi} \right)^{\frac{1}{3}} \quad (2)$$

where,  $D_{eq}$  equivalent diameter of the bubble,  $V_{vapor}$  vapor volume.

Table 3. Mesh structures are used in the computational domain.

Mesh Structure	Number of Nodes	Number of Cells
1	5752	5602
2	12847	12651
3	23121	22953

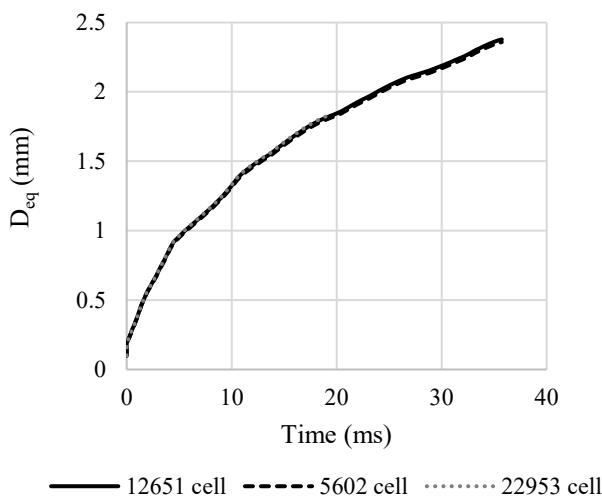


Figure 6. Mesh independence test.

Since the maximum difference in equivalent bubble growth diameters is released in Figure 6, all curves almost overlap entirely, indicating minimal variation. As shown in Table 4, the difference between the mesh configurations is less than 1%, highlighting the negligible impact of mesh size on the equivalent diameter. The simulations were continued using Mesh Structure 2 to optimize computational load and processing time.

Table 4. The % variation in the equivalent diameter of the bubble across different mesh structures.

Mesh Structure	$D_{eq}$ (mm)	Variation (%)
12651 cells	1,825	0
5602 cells	1,811	-0,8
22953 cells	1,837	0,5

It is well established in nucleate pool boiling processes that the heat transfer mechanism is primarily governed by natural convection. In line with this, previous studies have reported that the average flow velocity within the system can reach approximately 0.5 m/s [22]. It can be seen in Figure 7, which presents the CFD results of the velocity distribution from the copper plate surface to the atmospheric boundary, that the flow behavior is consistent with findings from the literature.

For the accuracy and stability of numerical solutions, the Courant number ( $Co$ ), a critical parameter, was set to 0.5 in this study. This value lies within a commonly accepted safe range for selecting the time step in transient simulations [24]. Considering that the minimum cell size around the cavity was 10 micrometers ( $10^{-5}$  m), the time step ( $\Delta t$ ) was initially estimated using the following relation [6]:

$$\Delta t = \frac{Co \cdot \Delta x}{u_{max}} = \frac{0.5 \times 10^{-5}}{3.5} = 1.47 \times 10^{-6} \quad (3)$$

However, to enhance the numerical stability of the solution, the time step was increased by one order of magnitude and applied as  $\Delta t = 1 \times 10^{-5}$  s. This value is consistent with those used in the literature for low Reynolds number boiling problems [24]

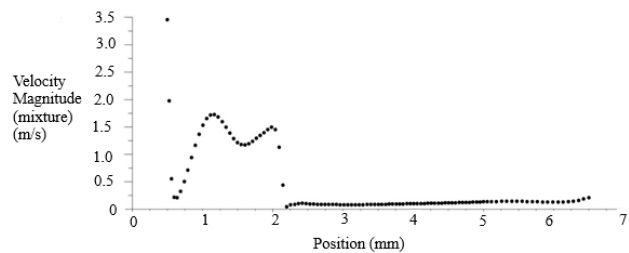


Figure 7. Velocity distribution from the copper plate surface to atmospheric pressure.

### 3.1. Governing Equations

The fluid flow analysis in this study is based on a series of simplifying assumptions and numerical methods designed to make the computational model both manageable and effective. Initially, the flow is assumed to be stagnant and at saturation temperature, providing a baseline for understanding the boiling dynamics. A two-dimensional axisymmetric model is employed using cylindrical coordinates, which reduces computational complexity while capturing the essential physics of the problem. The assumption of axial symmetry further streamlines the analysis by allowing focus on radial and axial components of the flow. Due to the relatively low velocities, the flow is modeled as laminar, eliminating the need to account for turbulence. The working fluids, water and vapor, are treated as Newtonian and incompressible, while their thermophysical properties are modeled as temperature-dependent to reflect realistic behavior. Surface tension effects and lift forces resulting from density gradients are also considered, enhancing the model's fidelity [21], [25].

Georgoulas and Marengo's study [26] contributes to understanding saturated pool boiling by developing and validating a diabatic CFD model based on the VOF method. This model accurately accounts for phase change due to evaporation and shows strong agreement with analytical and experimental data. It is further used to analyze the impact of key parameters on bubble growth, particularly on detachment diameter and time. The enhanced VOF interface-capturing approach is shown to be a promising and reliable tool for simulating various phase-change phenomena. In light of these findings, the present study the Volume of Fluid (VOF) method is adopted for tracking the liquid-vapor interface in the two-phase flow, and a User Defined Function (UDF) is integrated to represent heat input and boundary conditions more accurately. The CLSVOF method is employed to improve interface capturing further. This

approach leverages the strengths of both VOF and Level Set methods by reconstructing the interface through vectors perpendicular to it, derived from both functions. This reconstruction ensures improved mass conservation while maintaining an accurate and smooth interface representation. Although these assumptions and methods introduce certain limitations, they are essential for maintaining computational tractability and achieving meaningful, predictive insights into the boiling process.

According to Mudawar et al. [27], mass conservation for each phase is formulated by considering both the time-dependent variation and the convective transport (advection) of the phase's volume fraction. This conservation is balanced by the net mass exchange resulting from phase change processes, specifically the mass entering or leaving a computational cell. In this context, each phase's continuity is governed by fluid motion and interfacial mass transfer mechanisms such as evaporation and condensation, which directly affect the evolution of the volume fraction field. Here are the equations [27],

$$\frac{\partial \alpha_f}{\partial t} + \nabla \cdot (\alpha_f \vec{u}_f) = \frac{1}{\rho_f} \sum (\dot{m}_{gf} - \dot{m}_{fg}) \quad (4)$$

$$\frac{\partial \alpha_g}{\partial t} + \nabla \cdot (\alpha_g \vec{u}_g) = \frac{1}{\rho_g} \sum (\dot{m}_{fg} - \dot{m}_{gf}) \quad (5)$$

In this formulation,  $\alpha$  represents the volume fraction of the phase,  $t$  denotes time, and  $\vec{u}$  is the velocity vector describing fluid motion. The symbol  $\rho$  corresponds to the density of the phase, while  $\dot{m}$  indicates the mass transfer rate associated with phase change processes. Specifically,  $\dot{m}_{fg}$  refers to the mass transfer rate from liquid to vapor during evaporation, and  $\dot{m}_{gf}$  represents the reverse process, condensation, where vapor converts back to liquid.

A distinctive feature of the CLSVOF method is its explicit incorporation of surface tension forces directly into the momentum equation, distinguishing it from the conventional VOF approach. Despite this enhancement, the CLSVOF method, similar to the VOF method, solves a single momentum equation for the entire fluid domain by treating the system as a mixture. This is achieved through effective (pseudo-mixture) fluid properties, such as density and viscosity, which are calculated based on the local volume fractions of the involved phases. The resulting momentum equation governs the flow behavior across the interface and within both phases, ensuring a unified treatment of the multiphase domain. The equation is shown below [27],

$$\frac{\partial}{\partial t} (\rho \vec{u}) + \nabla \cdot (\rho \vec{u} \vec{u}) = -\nabla P + \nabla \cdot [\mu (\nabla \vec{u} + \nabla \vec{u}^T)] - \sigma \kappa \delta(\varphi) \nabla \varphi + \vec{S}_M \quad (6)$$

In this formulation,  $\sigma$  denotes the surface tension coefficient,  $\kappa$  represents the interface curvature, and  $\varphi$  refers to the Level-Set function used to track the interface position. The symbol  $P$  stands for pressure,  $\mu$  is the dynamic viscosity, and  $\vec{S}_M$  denotes the momentum source term accounting for interfacial forces such as surface tension. As the current study is conducted under zero-gravity (microgravity) conditions, the gravitational body force term is omitted from the momentum equation, simplifying the force balance on the fluid.

Similarly, the energy conservation equation employed in the CLSVOF method follows the same formulation as the conventional VOF approach. It governs the thermal transport within the multiphase system and accounts for both convection and conduction and latent heat effects due to phase change. The equation regarding effective mixture properties is expressed and ensures energy conservation across the liquid-vapor interface during evaporation and condensation processes. Here is the equation [27],

$$\frac{\partial}{\partial t} (\rho E) + \nabla \cdot (\vec{u} (\rho E + P)) = \nabla \cdot (k_{eff} \nabla T) + S_E \quad (7)$$

where,  $E$  denotes the internal energy of the fluid,  $\nabla T$  represents the temperature field, and  $k_{eff}$  is the effective thermal conductivity, which accounts for both liquid and vapor phases based on their local volume fractions. The term  $S_E$  refers to the volumetric heat source term, which incorporates the effects of phase change. Specifically,  $S_E$  is calculated as the product of the mass transfer rate due to phase change and the latent heat of vaporization, thereby capturing the energy exchange associated with evaporation and condensation processes at the phase interface.

In this study, a UDF was developed for simulations based on the CLSVOF method, aiming to perform time-dependent (transient) analyses involving evaporation, condensation, and bubble dynamics. The developed UDF was integrated into ANSYS Fluent to enhance the realistic modeling of multiphase flow and phase change processes. Each function within the UDF serves a specific purpose: Mass transfer processes between the liquid and gas phases are governed by a custom model that calculates evaporation and condensation rates based on local temperature and volume fraction data. The contact angle is dynamically updated at the end of each time step based on the computed bubble diameter and applied as a boundary condition. Critical parameters such as bubble diameter and departure diameter are also calculated and recorded in external files to facilitate post-processing and result evaluation.

#### 4. Results and Discussion

When a vapor bubble forms on a heated surface, it initially undergoes rapid growth. This growth rate, however, gradually decreases due to the downward movement of the surrounding liquid and the thermal boundary layer that develops around the bubble interface. Once the bubble reaches its maximum diameter, its base begins to contract, leading to detachment through a process known as vapor necking. After detachment, a portion of the vapor remains adhered to the surface. This residual vapor is a nucleation site for subsequent bubbles, sustaining the boiling cycle. Significantly, this remaining vapor inhibits complete rewetting of the surface area previously occupied by the bubble, which enhances and facilitates continued nucleation.

As shown in Figure 8, Tetik [28] examined the bubble nucleation cycle under a heat flux of 30 kW/m<sup>2</sup> and a wall superheat of 5.8 °C on surfaces containing micro-scale cavities. The experiments demonstrated that the base of the bubble remains anchored at the mouth of the cavity throughout much of the growth process. As the base expands, the effective area for evaporation increases, thereby enhancing heat transfer. The adhesive forces that retain the bubble within the cavity are relatively strong, necessitating a more significant buoyant force to trigger detachment.

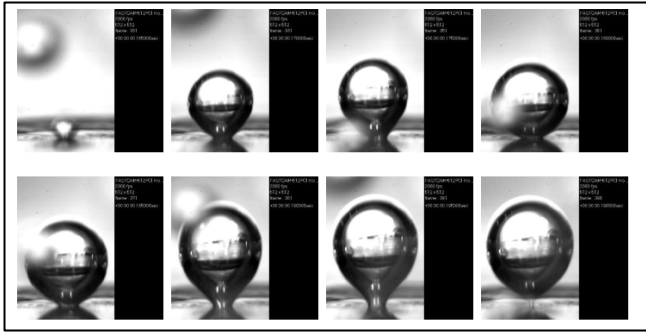
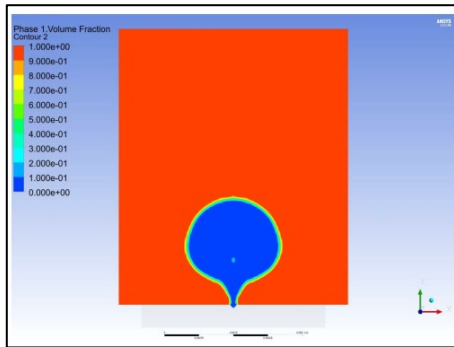


Figure 8. Bubble nucleation cycle in the cavity ( $q''=30 \text{ kW/m}^2$ ,  $\Delta T=5.8 \text{ }^\circ\text{C}$ ) [28].

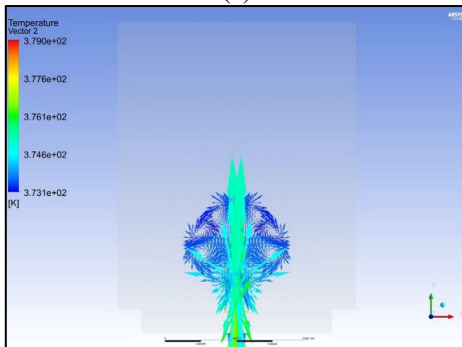
This force requirement is only met when sufficient vapor accumulates, resulting in a larger bubble departure diameter. These findings highlight the critical role of cavity geometry and surface characteristics in governing bubble behavior and heat transfer performance during nucleate boiling.

Figure 9a illustrates the formation of bubbles in a saturated water pool subjected to a heat flux of  $30 \text{ kW/m}^2$ , while Figure 9b presents the corresponding temperature gradients alongside color-coded velocity vectors. The velocity vectors in Figure 9b depict the movement of liquid as it rushes into the space vacated by the detaching bubble. This inflow exerts a downward force on the bubble, suspending it temporarily and facilitating the formation of a new, smaller bubble at the nucleation site. The first bubble rises during the necking phase, consistent with the experimental images shown in Figure 8.

Throughout the simulations, the residuals were closely monitored. As the analysis is transient, achieving steady-state convergence at each time step is unnecessary. Nevertheless, for the sake of numerical accuracy and stability, it was ensured that the residuals decreased to at least the order of  $1e-6$  during each time step.



(a)



(b)

Figure 9. a) The formation of bubbles in a saturated water pool subjected to a heat flux of  $30 \text{ kW/m}^2$ . b) Temperature gradients with color-coded velocity vectors.

Figure 10 compares the stages of bubble formation at a heat flux of  $30 \text{ kW/m}^2$ , as obtained from simulations, with corresponding Tetik's experimental observations under identical conditions [28]. Within a specific heat flux range, natural surface cavities or engineered cavities of varying shapes and sizes can effectively act as nucleation sites, provided they meet the minimum nucleation radius and possess sufficient vapor-holding capacity. At elevated heat fluxes, the increasing temperature difference activates more nucleation sites, each satisfying the critical nucleation radius requirement. As a result, the density of active sites on the boiling surface rises significantly, complicating the direct observation and measurement of individual bubble dynamics. The parameter, the number of active nucleation sites per unit area of the heating surface, is defined as the *effective nucleation site density*. A CFD analysis was performed at a base heat flux of  $30 \text{ kW/m}^2$  and extended to higher heat flux levels to investigate this phenomenon further. The numerical results obtained from these simulations were compared with experimental data, providing valuable insights into bubble dynamics, heat transfer performance, and the influence of heat flux on nucleation site activation.

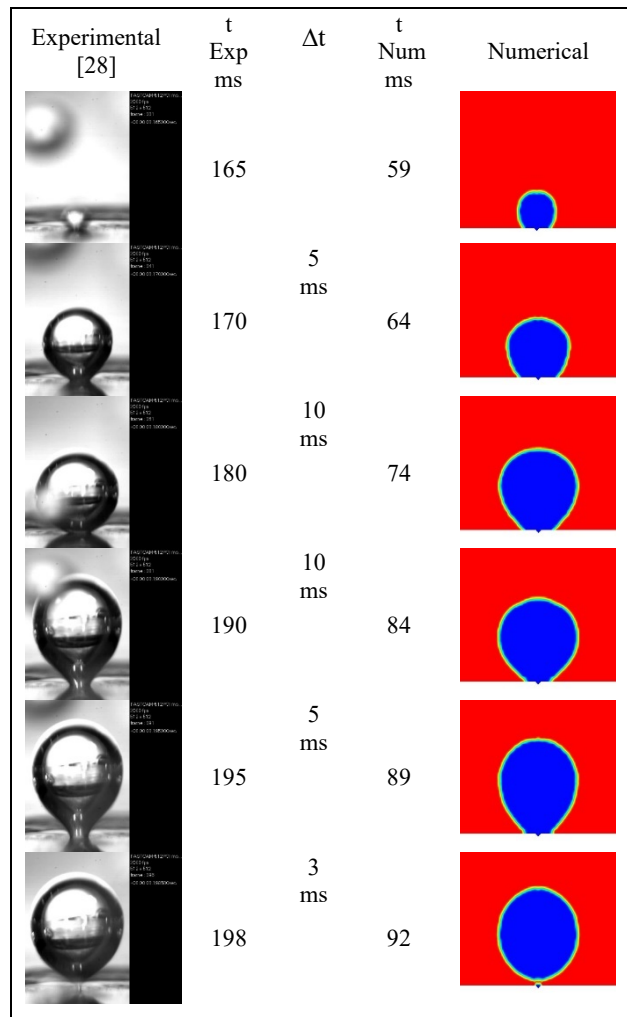


Figure 10. Bubble formation stages at a heat flux of  $30 \text{ kW/m}^2$  compared with Tetik's experimental observations at the same heat flux [28].

Figure 10 presents a 33-millisecond cycle, from 165 ms to 198 ms, using images obtained from Tetik's experimental study conducted at a heat flux of  $30 \text{ kW/m}^2$ . It is evident from the first image that these images do not correspond to the

initial bubble, as another bubble can be seen rising behind a newly forming one. Additionally, the time annotations shared alongside the experimental visuals do not represent the first bubble cycle; therefore, it is more appropriate to emphasize that the time intervals between frames are in the millisecond range. The numerical model aligned the initial simulation time with Tetik's 165-ms frame. Accordingly, the visualization of the CFD results begins at 59 ms and ends at 92 ms, completing a 33-millisecond cycle similar to that in Tetik's study. The results exhibit high similarity when CFD images are extracted at the same time intervals (5-10-10-5-3 ms).

A CFD analysis was performed at a base heat flux of 30 kW/m<sup>2</sup> and extended to higher heat flux levels to investigate this phenomenon further. The numerical results obtained from these simulations were compared with experimental data, providing valuable insights into bubble dynamics, heat transfer performance, and the influence of heat flux on nucleation site activation. Figure 11 presents the time evolution of vapor bubble diameter on a heated surface subjected to varying heat flux levels of 30, 60, 84, 122, and 177 kW/m<sup>2</sup>. The results demonstrate that increasing heat flux accelerates bubble growth, shortens the growth duration, and prompts earlier detachment. At the highest heat flux of 177 kW/m<sup>2</sup>, the bubble attains a diameter of approximately 2 mm in under 0.025 seconds before detaching. In contrast, at 30 kW/m<sup>2</sup>, the bubble reaches a larger diameter of 2.1 mm but detaches much later, around 0.088 seconds. Bubble formation is relatively slow at lower heat fluxes (e.g., 30 kW/m<sup>2</sup>). In contrast, higher heat fluxes (e.g., 177 kW/m<sup>2</sup>) promote rapid vapor generation, resulting in faster bubble growth. This behavior aligns well with the literature, where it is reported that higher heat flux enhances nucleation site activation and vapor generation rate, thereby increasing the bubble departure diameter and frequency [22], [23].

These findings are consistent with the theoretical analyses presented by Kandlikar [23], who emphasized the role of surface heat flux in determining bubble dynamics and departure characteristics. Similarly, Dhir [22] highlighted that elevated heat flux significantly impacts bubble growth time, contact diameter, and overall boiling heat transfer mechanisms. The present numerical results support these conclusions, reinforcing the model's validity. This behavior is consistent with the physical expectation that higher heat flux increases local wall superheat, enhancing vapor generation rates at the nucleation site [30], [31]. The observed bubble growth trends align well with classical boiling theory and previous experimental studies. For instance, Klausner et al. [31] and Dhir [32] have shown that increased thermal input accelerates phase change, leading to more rapid bubble expansion and decreased residence time on the surface. Additionally, numerical simulations by Bhati and Paruya [33] confirm that the growth rate and the maximum bubble diameter strongly depend on the applied heat flux, particularly during the early stages of nucleate boiling. These findings validate the accuracy of the CFD model employed in the current study and confirm its ability to reproduce realistic bubble dynamics under varying thermal conditions. As the heat flux rises, vertical bubble coalescence becomes more prevalent. The increasing temperature difference leads to faster bubble growth and more significant interaction between consecutive bubbles. When the upward velocity of a newly forming bubble at a nucleation site exceeds that of the preceding bubble, the two bubbles tend to coalesce vertically.

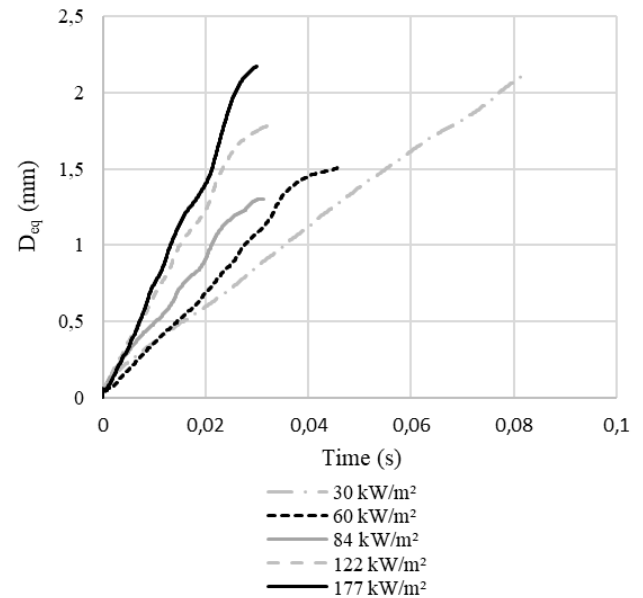


Figure 11. Bubble growth behavior under varying heat fluxes.

In such instances, the second bubble is rapidly drawn away from the surface and quickly merges with the first bubble. Although the rise velocity is relatively independent of the temperature difference, higher heat flux intensifies the vapor generation rate and promotes faster bubble expansion. Consequently, the frequency and intensity of bubble-bubble interactions increase, further influencing the boiling dynamics. As the heat flux increases, the dynamics of bubble formation during boiling undergo significant changes. An increased heat flux enhances the evaporation rate at the heating surface, leading to a higher bubble generation frequency. Initially, this results in larger bubble diameters due to the greater energy input; however, bubble size tends to decrease beyond a certain threshold. Zuber [34] demonstrated that bubbles detach more rapidly from the surface at high heat flux levels, preventing them from growing to larger sizes. Similarly, Lienhard and Dhir [35] observed that bubble diameter increases with moderate heat flux but decreases at higher values due to reduced residence time and intensified bubble interactions. Thus, the relationship between heat flux and bubble size is nonlinear: bubble diameter increases at low to moderate heat fluxes but decreases when heat input becomes excessive.

As the heat flux increases, vapor bubbles coalesce in the vertical direction, strongly influenced by the rising wall superheat. The elevated temperature difference accelerates the bubble growth rate. In contrast, the dynamics of a newly forming bubble are increasingly affected by the movement of the previously detached bubble from the same nucleation site. This interaction is illustrated in Figure 12, which shows sequential images captured at a heat flux of 60 kW/m<sup>2</sup>. Buyevich and Webbon [29] reported that such coalescence can form vapor columns, hindering the access of relatively cooler liquid to the surface and triggering the onset of critical heat flux.

With increasing heat flux and surface superheat, more nucleation sites become active. As the density of active nucleation sites and the frequency of bubble formation increase, interactions among neighboring bubbles become more prominent, leading to coalescence in both horizontal and vertical directions, as depicted in Figure 13.

When vapor bubbles of similar growth rates form at adjacent nucleation sites, horizontal coalescence occurs symmetrically. However, if bubbles form at different rates or with varying waiting times, they tend to merge at skewed angles. In cases where two bubbles form consecutively at the same nucleation site within a short time interval, vertical coalescence occurs. Here, the microlayer formed beneath the initially growing bubble rapidly evaporates, particularly when the first bubble remains attached to the surface. A thin liquid network layer can be observed between the bubbles, and the second bubble, forming beneath the first, quickly merges and assists in lifting the combined structure away from the surface. These observations underscore the complex interactions between bubble dynamics and cavity geometry. Within specific heat flux ranges, naturally occurring surface and engineered cavities with varying shapes and dimensions act as effective boiling sites, provided they satisfy the critical nucleation radius and possess sufficient vapor retention capability.

At elevated heat flux levels, the increase in wall superheat enhances the fulfillment of the critical nucleation radius criterion, activating more nucleation sites on the boiling surface. This proliferation of active boiling sites, or *effective boiling foci*, makes directly observing and measuring individual bubble dynamics increasingly difficult.

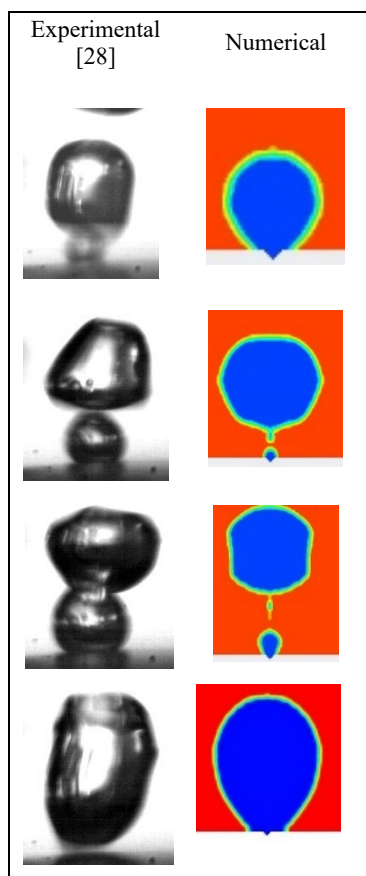


Figure 12. CFD result for  $60 \text{ kW/m}^2$ , mushroom-like shapes, Bubbles continuously coalescing in the vertical direction, compared to Tetik's experimental result ( $q''=60 \text{ kW/m}^2$ ) [28].

The density of these active sites, defined as the number of nucleation cavities per unit heating surface area where vapor bubbles form and grow, is referred to as the *effective boiling focus density*. Experimental studies have demonstrated that this density is influenced by several factors, including the applied heat flux, the wall superheat,

cavity geometry (such as diameter and depth), and the specific properties of the surface-fluid pair.

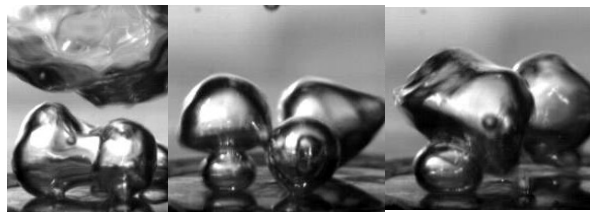


Figure 13. Events of bubbles merging in the vicinity of the boiling surface in horizontal, vertical, and diagonal axes [28].

Additionally, the spatial distribution and relative distances between active nucleation sites significantly affect bubble interactions, such as horizontal and vertical coalescence, which alter the overall boiling behavior and heat transfer performance.

In Figure 14, the variation of surface superheat ( $\Delta T$ ) as a function of heat flux ( $q''$ ) is presented comparatively based on both numerical modeling and Tetik's experimental data [28]. As can be seen from the figure, there is a strong agreement between the numerical and experimental results up to a heat flux of approximately  $122 \text{ kW/m}^2$ .

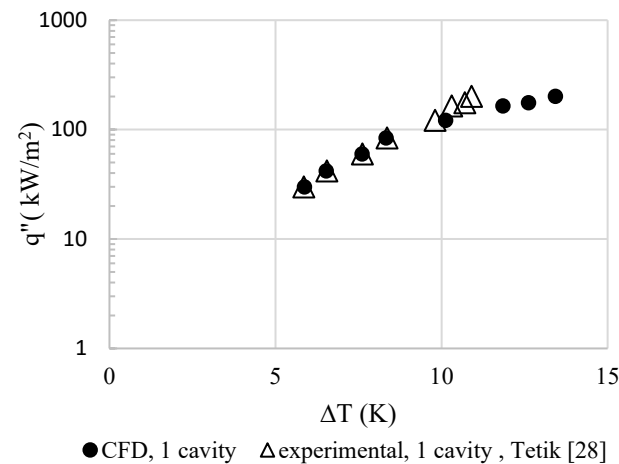


Figure 14. Heat flux-dependent surface temperatures: experimental and numerical measurement comparison.

However, this agreement starts to diverge beyond  $165 \text{ kW/m}^2$ , where a significant increase in surface superheat is observed in the numerical model compared to the experimental data. The primary reason for this discrepancy lies in the surface characteristics of the copper used in the experimental setup. Unlike the idealized geometry used in simulations, the real copper surface contains naturally occurring microscopic cavities that are not artificially engineered. These micro-cavities act as additional nucleation sites at high heat flux levels, enabling the formation of new vapor bubbles. This promotes more efficient heat removal through boiling and limits the rise in surface temperature [21],[36]. In contrast, the numerical model assumes a copper surface with a single artificial cavity of 150 microns in diameter, while the rest of the surface is modeled as perfectly smooth and flat. This restricts the formation of new nucleation sites, causing bubble generation to remain localized at a single point. As heat flux increases, this limitation results in higher surface superheat values in the simulation. Consequently, the discrepancy in surface

superheat between the two approaches becomes more pronounced when the heat flux exceeds a certain threshold, approximately 122 kW/m<sup>2</sup>.

Table 5. Comparison of experimental and numerical surface temperature (superheat) measurements under varying heat flux.

Heat Flux $q''$ (kW/m <sup>2</sup> )	$\Delta T$ (K), exp [28] 1 cavity	$\Delta T$ (K), CFD 1 cavity	$\Delta T$ (K), CFD Plain
30	5,85	5,87	7,16
42	6,54	6,52	8,61
60	7,61	7,60	9,73
84	8,35	8,33	10,82
122	9,8	10,12	13,47
165	10,3	11,84	15,64
177	10,7	12,61	16,11
202	10,9	13,42	17,22

Table 5 presents the surface superheat values obtained from the experimental study conducted by Tetik on a copper surface with a single cavity under varying heat flux conditions. Additionally, the table includes the surface superheat differences derived from the CFD simulations performed within the scope of this study for both a single-cavity copper surface and a plain copper surface. As can be seen in Figures 14 and 15b, the plain surface exhibits higher superheat values compared to the cavity surface, due to its lower boiling heat removal capability. Figure 14 illustrates the relationship between heat flux and surface superheat within the nucleate boiling regime.

In Figure 15a, the A-B region on Nukiyama's [37] classic boiling curve corresponds to the initial subregion of nucleate boiling, characterized by isolated bubble formation without the onset of slug flow. This subregion represents the early stages of efficient heat transfer, where individual vapor bubbles form and detach without significant bubble-bubble interaction. In Figure 15b, the experimental results obtained by Küçük [38] for a plain (smooth) copper surface are represented by circular markers. As the heat flux increases, the surface superheat values exhibit a nonlinear rise, characteristic of nucleate boiling behavior. The CFD results for the same plain copper surface are shown using cross markers. Regarding the CFD results for the single-cavity surface, the presence of the cavity enhances heat removal from the surface through boiling. As a result, the surface superheat remains lower than the CFD results for the plain surface and the experimental results reported by Küçük [38].

Since both datasets correspond to smooth surfaces, the results are in close agreement, demonstrating the CFD model's consistency and reliability. Triangle markers represent the CFD study conducted on a copper surface with a single cavity. Compared with the experimental results of Tetik [28] for a single-cavity copper surface in Figure 14, this dataset in the current graph emphasizes the difference in boiling performance between plain and cavity-enhanced surfaces. Due to the presence of the cavity, more nucleation sites are activated, which increases vapor bubble generation and enhances heat transfer by boiling. As a result, the surface superheat remains lower for the same heat flux values than the plain surface, and this difference is maintained across increasing heat flux levels. This observation also supports the conclusion drawn from Figure 14, where Tetik's experimental surface, although designed with a single cavity, may also contain natural micro-defects or pores that act as

additional nucleation sites. Consequently, more intense bubble activity occurs, drawing more heat from the surface and resulting in even lower surface superheat values than those predicted by the CFD model. After approximately 122 kW/m<sup>2</sup> heat flux, the divergence between the experimental and CFD results becomes more pronounced, further confirming this behavior.

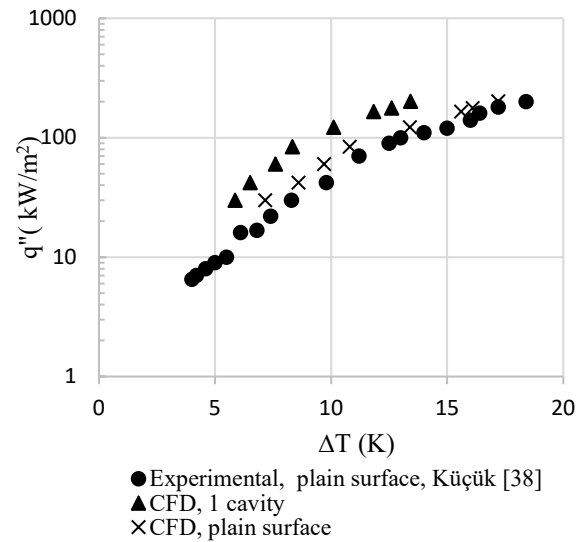
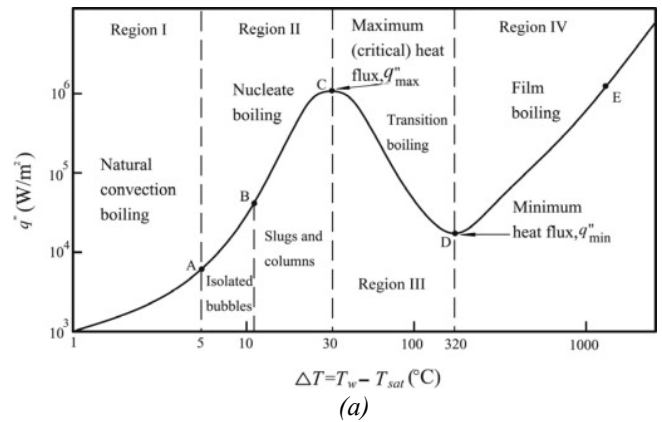


Figure 15. Surface superheat levels as a function of heat flux. a) Nukiyama Boiling Curve [37], b) Küçük's experimental result surface superheating levels dependent on heat flux [38], and surface superheat levels as a function of heat flux obtained from CFD results, both plain and one cavity surface.

## 5. Conclusion

This study has presented a detailed numerical investigation of saturated nucleate pool boiling on heated surfaces featuring a single micro-cavity. Using the VOF method in ANSYS Fluent, supported by a custom-developed UDF, the simulations successfully captured the key mechanisms of bubble nucleation, growth, coalescence, and detachment. The primary focus was on analyzing bubble geometry and departure diameter to understand boiling behavior at the microscale.

The simulation results agreed with experimental data reported in the literature, particularly with the studies referenced in [28] and [38], thereby validating the robustness and accuracy of the proposed numerical model. These validations strengthen confidence in using such models for predictive analysis of boiling performance on microstructured surfaces.

Based on the outcomes, it is strongly recommended that surface enhancement techniques, such as etching, coating, or creating structured cavities, be employed to improve boiling heat transfer efficiency significantly. Such modifications can increase the density of active nucleation sites, facilitate bubble departure, and reduce wall superheat. To highlight a few key findings from the study, the bubble growth rate accelerates as the heat flux increases. However, the behavior related to bubble diameter becomes more complex. Bubbles proliferate and detach before reaching large sizes, increasing the bubble departure frequency. The LEE boiling model was initially employed during the implementation of the CLSVOF method. Although boiling and bubble growth were observed on both a flat surface and a surface with cavities, bubble detachment from the surface did not occur. Therefore, using a User-Defined Function (UDF) is essential to capture a complete bubble life cycle accurately.

Future studies will extend the current work by incorporating various cavity geometries and configurations and will be conducted in three dimensions (3D). This approach aims to simulate boiling surfaces more realistically. These extended simulations will focus on gaining a deeper understanding of bubble interactions and their cumulative effects on overall heat transfer performance, ultimately contributing to the design of high-efficiency thermal management systems.

## Nomenclature

### Symbols

$Co$	Courant Number
$C_p$	Specific heat (J/kg·K)
$D_{eq}$	Equivalent diameter of the bubble (mm)
$E$	Internal energy (J)
$h$	Convective heat transfer coefficient (W/m <sup>2</sup> K)
$h_{fg}$	Latent heat of vaporization (kJ/kg)
$k$	Thermal conductivity (W/mK)
$k_{eff}$	Effective thermal conductivity (W/mK)
$\dot{m}$	Mass transfer rate (kg/m <sup>2</sup> s)
$\dot{m}_{fg}$	Mass transfer rate from liquid to vapor during evaporation (kg/m <sup>2</sup> s)
$\dot{m}_{gf}$	Mass transfer rate from vapor to liquid during condensation (kg/m <sup>2</sup> s)
$P$	Pressure (MPa)
$S_E$	Volumetric heat source term (W/m <sup>3</sup> )
$\vec{S}_M$	Momentum source term (N/m <sup>3</sup> )
$t$	Time (s)
$T_{sat}$	The saturation temperature of the liquid (K)
$T_w$	The temperature of the heated surface (K)
$\vec{u}$	Velocity vector (m/s)
$u_{max}$	Maximum velocity (m/s)
$V_{vapor}$	Vapor volume (mm <sup>3</sup> )

### Greek letters

$\alpha$	Volume fraction of the phase
$\Delta t$	Time step (s), (ms)
$\Delta T_e$	The excess temperature or superheat
$\Delta x$	Cell size ( $\mu$ m)
$\kappa$	Interface curvature (1/m)
$\mu$	Viscosity (Pa·s)
$\rho$	Density (kg/m <sup>3</sup> )
$\sigma$	Surface tension coefficient (N/m)
$\phi$	Level Set function
$\nabla T$	Temperature field (K)

## Subscripts

$f$	Liquid phase
$g$	Vapor phase

## Abbreviations

CFD	Computational Fluid Dynamics
CHF	Critical Heat Flux
CLSVOF	Coupled Level Set and Volume of Fluid
GRWBM	Grid Resolved Wall Boiling Model
HTC	Heat Transfer Coefficient
LBM	Lattice Boltzmann Method
LS	Level Set
PBHT	Pool Boiling Heat Transfer

## References:

- [1] A. Al-Nagdy, M. I. A. Habba, R. A. Khalaf-Allah, S. M. Mohamed, M. T. Tolan, and A. S. Easa, "Optimizing pool boiling heat transfer with laser-engineered microchannels: Experimental and RSM modeling analysis," *International Journal of Thermal Sciences*, vol. 213, 2025, Art. no. 109806, doi: 10.1016/j.ijthermalsci.2025.109806.
- [2] E. I. Eid, A. A. Al-Nagdy, and R. A. Khalaf-Allah, "Nucleate pool boiling heat transfer above laser machining heating surfaces with different micro-cavity geometric shape for water-aluminum oxide nanofluid," *Experimental Heat Transfer*, vol. 35, no. 5, pp. 688–707, Jul. 2022, doi: 10.1080/08916152.2021.1946207.
- [3] E. I. Eid, R. A. Khalaf-Allah, S. H. Taher, and A. A. Al-Nagdy, "An experimental investigation of the effect of the addition of nano Aluminum oxide on pool boiling of refrigerant 134A," *Heat and Mass Transfer*, vol. 53, pp. 2597–2607, 2017, doi: 10.1007/s00231-017-2010-y.
- [4] T. Chen and J. N. Chung, "Heat-transfer effects of coalescence of bubbles from various site distributions," *Proceedings of the Royal Society A: Mathematical, Physical and Engineering Sciences*, vol. 459, 2003, doi:10.1098/rspa.2003.1133.
- [5] A. Coulibaly, X. P. Lin, J. L. Bi, and D. M. Christopher, "Effect of bubble coalescence on the wall heat transfer during subcooled pool boiling," *International Journal of Thermal Sciences*, vol. 76, pp. 101–109, 2014, doi: 10.1016/j.ijthermalsci.2013.08.019.
- [6] T. L. Bergman, A. S. Lavine, F. P. Incropera, D. P. Dewitt, *Fundamentals of Heat and Mass Transfer*, 8th Edition, John Wiley & Sons, 2018.
- [7] Y. Y. Hsu, "On the size range of active nucleation cavities on a heating surface," *ASME Journal of Heat and Mass Transfer*, pp. 207–213, 1962, doi:10.1115/1.3684339.
- [8] M. K. Gupta, D. S. Sharma, and V. J. Lakhera, "Vapor bubble formation, forces, and induced vibration: A review," *ASME Applied Mechanics Reviews*, vol. 68, 2016, Art. no. 030801, doi:10.1115/1.4033622.
- [9] D. B. R. Kenning, "Nucleate Boiling," in *Thermopedia*. Begell House Inc., 2011, doi: 10.1615/AtoZ.n.nucleate\_boiling

- [10] S. Paruya, J. Bhati, and F. Akhtar, "Numerical model of bubble shape and departure in nucleate pool boiling," *International Journal of Heat and Mass Transfer*, vol. 180, 2021, Art. no. 121756, doi: 10.1016/j.ijheatmasstransfer.2021.121756.
- [11] M. M. Petrovic and V. D. Stevanovic, "Pool boiling simulation with two-fluid and grid resolved wall boiling model," *International Journal of Multiphase Flow*, vol. 144, 2021, Art. no. 103806, doi: 10.1016/j.ijmultiphaseflow.2021.103806.
- [12] S. Iyer, A. Kumar, J. Coventry, and W. Lipiński, "Modelling of bubble growth and detachment in nucleate pool boiling," *International Journal of Thermal Sciences*, vol. 185, 2023, Art. No. 108041, doi: 10.1016/j.ijthermalsci.2022.108041.
- [13] M. M. Mahmoud and T. G. Karayiannis, "Bubble growth models in saturated pool boiling of water on a smooth metallic surface: Assessment and a new recommendation," *International Journal of Heat and Mass Transfer*, vol. 208, 2023, doi: 10.1016/j.ijheatmasstransfer.2023.124065.
- [14] A. A. Alsaati, D. M. Warsinger, J. A. Weibel, and A. M. Marconnet, "A mechanistic model to predict saturated pool boiling critical heat flux (CHF) in a confined gap," *International Journal of Multiphase Flow*, 2023, Art. no. 104542, doi: 10.1016/j.ijmultiphaseflow.2023.104542.
- [15] N. Qiu, Y. Xuan, J. Li, and Q. Li, "Numerical simulation of nucleate pool boiling under high pressure using an initial micro-layer thickness model," *Case Studies in Thermal Engineering*, vol. 39, 2022, Art. no. 102460, doi: 10.1016/j.csite.2022.102460.
- [16] N. Kumar, P. Ghosh, and P. Shukla, "Development of an approximate model for the prediction of bubble departure diameter in pool boiling of water," *International Communications in Heat and Mass Transfer*, vol. 127, 2021, Art. no. 105531, doi: 10.1016/j.icheatmasstransfer.2021.105531.
- [17] M. Kim and S. J. Kim, "A mechanistic model for nucleate pool boiling including the effect of bubble coalescence on area fractions," *International Journal of Heat and Mass Transfer*, vol. 163, 2020, Art. no. 120453, doi: 10.1016/j.ijheatmasstransfer.2020.120453.
- [18] J. Yuan, X. Ye, and Y. Shan, "Modeling of the bubble dynamics and heat flux variations during lateral coalescence of bubbles in nucleate pool boiling," *International Journal of Multiphase Flow*, vol. 142, 2021, Art. no. 103701, doi: 10.1016/j.ijmultiphaseflow.2021.103701.
- [19] A. Mukherjee and V. K. Dhir, "Study of lateral merger of vapor bubbles during nucleate pool boiling," *ASME Journal of Heat and Mass Transfer*, vol. 126, pp. 1023–1039, 2004, doi:10.1115/1.1834614.
- [20] ANSYS Inc., ANSYS Fluent User's Guide, Release 2023 R1, Canonsburg, PA, USA, 2023.
- [21] S. V. Patankar, *Numerical Heat Transfer and Fluid Flow*, Washington, D.C.: Hemisphere Publishing Corporation, 1980, doi:10.1201/9781482234213.
- [22] V. K. Dhir, "Boiling heat transfer," *Annual Review of Fluid Mechanics*, vol. 30, no. 1, pp. 365–401, 1998, doi: 10.1146/annurev.fluid.30.1.365.
- [23] S. G. Kandlikar, "A theoretical model to predict pool boiling CHF incorporating effects of contact angle and orientation," *ASME Journal of Heat and Mass Transfer*, vol. 123, no. 6, pp. 1071–1079, 2001, doi:10.1115/1.1409265.
- [24] J. H. Ferziger and M. Perić, *Computational Methods for Fluid Dynamics*, 3<sup>rd</sup> edition, Springer, 2002.
- [25] J. G. Collier and J. R. Thome, *Convective Boiling and Condensation*, 3<sup>rd</sup> edition, Oxford, UK: Oxford University Press, 1994.
- [26] A. N. Georgoulas, M. Marengo, "Numerical Simulation of Pool Boiling: The Effects of Initial Thermal Boundary Layer, Contact Angle and Wall Superheat," in *Proc. 14th UK Heat Transfer Conference (UKHTC)*, Belfast, UK, 2015.
- [27] I. Mudawar, S. Kim, and J. Lee, "A coupled level-set and volume-of-fluid (CLSVOF) method for prediction of microgravity flow boiling with low inlet subcooling on the International Space Station," *International Journal of Heat and Mass Transfer*, vol. 202, 2023, Art. no. 124644, doi: 10.1016/j.ijheatmasstransfer.2023.124644.
- [28] T. Tetik, "Study of Bubble Nucleation in a Microcavity in Pool Boiling", Ph.D. Thesis, Dept. Mech. Eng., Tech. Univ. Istanbul, Graduate School of Science Eng. and Tech., Turkey, 2022.
- [29] Y. A. Buyevich and B. W. Webbon, "The isolated bubble regime in pool nucleate boiling," *International Journal of Heat and Mass Transfer*, vol. 40, issue 2, pp. 365–377, 1997, doi:10.1016/0017-9310(96)00097-X.
- [30] M. G. Cooper, "Heat flow rates in saturated nucleate pool boiling - a wide-ranging examination using reduced properties," *Advances in Heat Transfer*, vol. 16, pp. 157–239, 1984, doi: 10.1016/S0065-2717(08)70205-3.
- [31] J. F. Klausner, R. Mei, D. M. Bernhard, and L. Z. Zeng, "Vapor bubble departure in forced convection boiling," *International Journal of Heat and Mass Transfer*, vol. 36, issue 3, pp. 651–662, 1993, doi:10.1016/0017-9310(93)80041-R.
- [32] V. K. Dhir, "Mechanistic Prediction of Nucleate Boiling Heat Transfer—Achievable or a Hopeless Task?," *ASME Journal of Heat and Mass Transfer*, vol. 128, pp. 1–12, 2006, doi:10.1115/1.2136366.
- [33] J. Bhati, S. Paruya, "Numerical simulation of bubble dynamics in pool boiling at heated surface," *International Journal of Heat and Mass Transfer*, vol. 152, 2020, Art. no. 119465, doi: 10.1016/j.ijheatmasstransfer.2020.119465.
- [34] N. Zuber, "Hydrodynamic aspects of boiling heat transfer," Thesis, *U.S. Department of Energy Office of Scientific and Technical Information*, 1959, doi:10.2172/4175511.

- [35] J. H. Lienhard, V. K. Dhir, "Extended hydrodynamic theory of the peak and minimum pool boiling heat fluxes," *NASA Technical Report CR-2270*, 1973.
- [36] M. Mobli, C. Li, "On the heat transfer characteristics of a single bubble growth and departure during pool boiling," *ASME 2016 14th International Conference on Nanochannels, Microchannels, and Minichannels*, Washington, 2016, doi: 10.1115/ICNMM2016-8097.
- [37] S. Nukiyama, "The maximum and minimum values of the heat Q transmitted from metal to boiling water under atmospheric pressure," *International Journal of Heat and Mass Transfer*, vol. 9, pp. 1419-1433, 1966, doi: 10.1016/0017-9310(66)90138-4.
- [38] H. Küçük, "Effect of Solid Particles on Heat Transfer in Nucleate Pool Boiling", Ph.D. Thesis, Dept. Mech. Eng., Tech. Univ. Istanbul, Graduate School of Science Eng. and Tech., Turkey, 2002.